

Effect of elongational flow on ferrofluids under a magnetic field

S. Altmeyer* and Younghae Do†

Department of Mathematics, Kyungpook National University, Daegu 702-701, Korea

J. M. Lopez‡

School of Mathematical and Statistical Sciences, Arizona State University, Tempe, Arizona 85202, USA

(Received 21 January 2013; revised manuscript received 22 May 2013; published 8 July 2013)

To set up a mathematical model for the flow of complex magnetic fluids, noninteracting magnetic particles with a small volume or an even point size are typically assumed. Real ferrofluids, however, consist of a suspension of particles with a finite size in an almost ellipsoid shape as well as with particle-particle interactions that tend to form chains of various lengths. To come close to the realistic situation for ferrofluids, we investigate the effect of elongational flow incorporated by the symmetric part of the velocity gradient field tensor, which could be scaled by a so-called *transport coefficient* λ_2 . Based on the hybrid finite-difference and Galerkin scheme, we study the flow of a ferrofluid in the gap between two concentric rotating cylinders subjected to either a transverse or an axial magnetic field with the transport coefficient. Under the influence of a transverse magnetic field with $\lambda_2 = 0$, we show that basic state and centrifugal unstable flows are modified and are inherently three-dimensional helical flows that are either left-winding or right-winding in the sense of the azimuthal mode-2, which is in contrast to the generic cases. That is, classical modulated rotating waves rotate, but these flows do *not*. We find that under elongational flow ($\lambda_2 \neq 0$), the flow structure from basic state and centrifugal instability flows is modified and their azimuthal vorticity is linearly changed. In addition, we also show that the bifurcation threshold of the supercritical centrifugal unstable flows under a magnetic field depends linearly on the transport coefficient, but it does not affect the general stabilization effect of any magnetic field.

DOI: [10.1103/PhysRevE.88.013003](https://doi.org/10.1103/PhysRevE.88.013003)

PACS number(s): 47.20.Ky, 47.65.Cb

I. INTRODUCTION

There has been much interest recently in the use of ferrofluids [1] due to a wide variety of applications, ranging from their use in computer hard drives to their use in laboratory experiments to study geophysical flows [2,3]. A fundamental understanding of their magnetohydrodynamics is essential in order to better exploit their potentials. Ferrofluids are manufactured fluids consisting of dispersion of magnetized nanoparticles in a variety of liquid carriers, which can be stabilized against agglomeration by the addition of a surfactant monolayer onto the particles. In the absence of a magnetic field, the magnetic nanoparticles are randomly orientated, the fluid has zero net magnetization, and the presence of the nanoparticles only slightly alters the fluid's viscosity and density. When applying a sufficiently strong magnetic field, the ferrofluid flows toward regions of the magnetic field, and the hydrodynamics properties such as the viscosity can be significantly changed [4,5].

When describing the hydrodynamics of ferrofluids, it is assumed that the particles aggregate to form clusters having the form of chains, and thus it hinders the free flow of the fluid and increases the viscosity [6–8]. In this type of structure's formation, it is also assumed that the interaction parameter is usually greater than unity [1], thus the strength of the grain-grain interaction can be measured in terms of the total momentum of a particle.

For a magnetodissipative structure of ferrofluid dynamics, a different type of model equations [9] based on general principles is derived in which both the Debye theory [10] and the effective field theory by Shliomis [4,11] are included as special cases. In such a derivation for macroscopic ferrofluid dynamics, the magnetization's relaxation equation includes an additional term that is proportional to the product of the magnetization's magnitude and the symmetric part of the velocity gradient tensor, which can describe an elongational flow scaled by a so-called *transport coefficient* λ_2 . Such a term also exists in the dynamics of nematic liquid crystals as the flow alignment's effect on the director field in an applied shear flow [12].

The authors in Ref. [9] consider the term λ_2 as a material-dependent function of thermodynamic variables such as density, concentration, and temperature, but independent of shear. Then they show that λ_2 can be handled as a reactive transport coefficient which does not enter the expression for entropy production. In addition, by comparing the experimental measurement for the magnetovortical resonance [13,14], they estimated $\lambda_2 \approx 2.54$ for their used ferrofluid and for flow-induced modification of the relaxation time, and they argued that the shear flow induces fracture of dynamical particle chains, which leads to a reduced effective dipolar interaction between the particles.

For the nonequilibrium magnetization of the ferrofluid in the Taylor-Couette system for a simple stationary flow configuration subjected to a homogeneous transverse magnetic field, the first experiments [6,15] show that the symmetric part of the velocity gradient (i.e., the elongational flow component) is not zero. Thus, this result indicates that λ_2 significantly affects the magnetization vector in the ferrofluid on microstructural properties of the ferrofluid.

*sebastian_altmeyer@t-online.de

†yhdo@knu.ac.kr

‡jmlopez@asu.edu

For plane shear flow, the vorticity vanishes but the symmetric part of the velocity gradient tensor does not. Thus, for spherical particles, the relaxation of magnetization is not affected. This implies that λ_2 is equal to zero. In contrast, for elongated structures, such flows produce a radial gradient of angular momentum acting on the structures, which will alter the relaxation of magnetization of the fluid. In particular, considering the impact of particle-particle interaction of fluids, the term λ_2 is not zero. For instance, in Refs. [6,15], nonzero λ_2 was estimated: $0 < \lambda_2 \lesssim 0.88$, which depends on the used ferrofluid. Numerical analyses of the linearized Navier-Stokes equations with pure axial applied magnetic field suggest that the term λ_2 can modify the bifurcation threshold of primary instabilities [25].

In this paper, with the aim of investigating the influence of elongational flow effects, we do direct numerical simulations, which correspond to the experiments reported in Refs. [6,15], in a finite length Taylor-Couette system ($\Gamma = 20$) enclosed by stationary end walls with an outer cylinder mostly at rest. Here, parameter regimes and material properties of the ferrofluids used in the cited experiments are used.

The paper is subdivided into four parts. Following the introduction, Sec. II describes the model system for the magnetization including λ_2 and methods of investigation. It presents the velocity field and describes the implications of the magnetic terms in the generalized Navier-Stokes equations. In Secs. III and IV, we elucidate how the basic flow and the centrifugal instability are influenced under a finite transport coefficient λ_2 in a transverse and an axial magnetic field, respectively, which are the main results of this paper. We focus on bifurcation properties and the spatiotemporal dynamics of the involved flow states. Further, we explain the enforcing and counteracting effect of λ_2 and the untouched stabilization effect of any applied magnetic field. Finally, Sec. V summarizes the main results and draws conclusions.

II. GOVERNING EQUATIONS AND NUMERICAL TECHNIQUE

Consider an incompressible, isothermal, homogeneous, monodispersed ferrofluid with kinematic viscosity ν and density ρ in the annular gap between two independent cylinders. The inner cylinder of radius R_1 rotates at angular speed ω , but the outer cylinder of radius R_2 is stationary. The end walls enclosing the annulus are stationary. The length-to-gap aspect ratio of the annulus and the radius ratio are fixed at $\Gamma = 20$ and $R_1/R_2 = 0.5$, respectively, which is a typically geometrical setting used in the experiments; see, e.g., [7]. Using the gap width $d = R_2 - R_1$ as the length scale, the diffusion time d^2/ν as the time scale, a scaling pressure with $\rho\nu^2/d^2$, the magnetic field \mathbf{H} , and the magnetization \mathbf{M} with $(\rho/\mu_0)^{0.5}\nu/d$, the nondimensional governing equations are

$$\begin{aligned} (\partial_t + \mathbf{u} \cdot \nabla)\mathbf{u} - \nabla^2\mathbf{u} + \nabla p &= (\mathbf{M} \cdot \nabla)\mathbf{H} + \frac{1}{2}\nabla \times (\mathbf{M} \times \mathbf{H}), \\ \nabla \cdot \mathbf{u} &= 0, \end{aligned} \quad (2.1)$$

where $\mathbf{u} = (u, v, w)$ is the velocity in the cylindrical polar coordinate system (r, θ, z) and its corresponding vorticity is (ξ, η, ζ) . Here, a homogeneous external magnetic field of strength H_x or H_z is imposed in either the transverse x direction or the axial z direction, respectively, where $x = r \cos \theta$

and μ_0 is the magnetic permeability of free space. For velocity boundary conditions, it is zero on all stationary boundaries, but on the rotating inner cylinder, $\mathbf{u}(r_1, \theta, z) = (0, \text{Re}, 0)$, where Re is the Reynolds number:

$$\text{Re} = \omega r_1 d / \nu. \quad (2.2)$$

The nondimensional inner and outer cylinder radii are $r_1 = R_1/(R_2 - R_1)$ and $r_2 = R_2/(R_2 - R_1)$, respectively.

Equation (2.1) is solved together with an equation that describes the magnetization of the ferrofluid. A generic approximation is to use the equilibrium magnetization of an unperturbed state with homogeneously magnetized ferrofluid at rest with the mean magnetic moments orientated in the direction of the magnetic field, $\mathbf{M}^{\text{eq}} = \chi \mathbf{H}$, where χ is the magnetic susceptibility of the ferrofluid, determined using Langevin's formula [16]. In this paper, our used ferrofluid corresponds to APG933 [17] with $\chi = 0.9$.

In our study, we have used the Niklas approximation [18–21] at near equilibrium with small $\|\mathbf{M} - \mathbf{M}^{\text{eq}}\|$ and small relaxation times $\Omega\tau \ll 1$, where $\Omega = \nabla \times \mathbf{u}/2$ is the vorticity, Ω is the absolute value, and τ is the magnetic relaxation time. To determine the relationship between the magnetization \mathbf{M} , the magnetic field \mathbf{H} , and the velocity \mathbf{u} , we may consider an additional dependence of the magnetization on the symmetric part of the velocity gradient $\mathbb{S} = \frac{1}{2}(\partial_i u_j + \partial_j u_i)$. Finally, we can get that

$$\mathbf{M} - \mathbf{M}^{\text{eq}} = c_N^2 \mathbf{F}, \quad (2.3)$$

where $\mathbf{F} = \Omega \times \mathbf{H} + \lambda_2 \mathbb{S} \mathbf{H}$ and $c_N^2 = \tau/(1/\chi + \tau\mu_0 H^2/6\mu\Phi)$ is the Niklas coefficient with the dynamic viscosity μ , the vacuum viscosity μ_0 , and the volume fraction Φ of the magnetic material.

Note that the relaxation time τ could typically be defined by $\tau = \tau_B \langle D^3 \rangle^{\frac{1}{3}}$, where τ_B is the Brownian relaxation time and $\langle D^3 \rangle^{\frac{1}{3}}$ is the averaged diameter of the magnetic particles. Here, to investigate the effect of elongational flow, we assume that τ is constant, which is independent of the magnetic field \mathbf{H} . Our used relaxation time in this paper is from the experimental result [17] ($\tau = \tau_{\text{APG933}}/\tau_D = 0.0018$).

Using Eq. (2.3), the magnetization part in Eq. (2.1) can be eliminated. We thus have the following ferrohydrodynamic equation of motion [9]:

$$\begin{aligned} (\partial_t + \mathbf{u} \cdot \nabla)\mathbf{u} + \nabla p_M - \nabla^2\mathbf{u} \\ = -\frac{c_N^2}{2} \{ \mathbf{H} \nabla \cdot \mathbf{F} + \mathbf{H} \times \nabla \times \mathbf{F} \}, \end{aligned} \quad (2.4)$$

where p_M is the dynamic pressure incorporating all magnetic terms which can be written as gradients, i.e., $\nabla(\mathbf{H} \cdot \mathbf{H})$ and $\nabla[(\mathbf{H}_{\text{eq}} - \mathbf{H}) \cdot \mathbf{M}]$.

In our numerical simulations, we assume that the internal magnetic field is equal to the external imposed magnetic field. It is known as a leading-order approximation [20] and sufficiently good for a “first” numerical investigation for the effect of elongational flow. Therefore, Eq. (2.4) can be simplified:

$$\begin{aligned} (\partial_t + \mathbf{u} \cdot \nabla)\mathbf{u} - \nabla^2\mathbf{u} + \nabla p_M \\ = s_N^2 \{ \nabla^2\mathbf{u} - 2\lambda_2 \nabla \cdot \mathbb{S} \mathbf{H} - \mathbf{H} \times [2\nabla \times (\Omega \times \mathbf{H}) \\ - \mathbf{H} \times \nabla^2\mathbf{u} + \lambda_2 \nabla \times \mathbb{S} \mathbf{H}] \}. \end{aligned} \quad (2.5)$$

In this approach, the magnetic field and all the magnetic properties of the ferrofluid could be influenced by the velocity field, the transport coefficient λ_2 , and the magnetic field (Niklas) parameter $\mathbf{s}_N^2 = s_i \mathbf{e}_i$, $i = x, z$, where $s_x = [2(2 + \chi)/(2 + \chi)^2 - \chi^2 \eta^2] H_x c_N$ and $s_z = H_z c_N$.

Note that in our approach, the transport coefficient λ_2 is just a number [9], which can be scaled by the term describing the elongational flow and is always independent of \mathbf{H} . Thus, it only appears in combination with the symmetric component of the velocity field tensor. However, in real ferrofluids an H dependence takes place in the microscopic aspect of the dynamics of ferrofluids with chains or nonspherical particles [24].

The ferrohydrodynamic system (2.5) is numerically solved with the code G1D3 [20,21], which combines a finite-difference method of second order in (r, z) and time (explicit) with Fourier spectral decomposition in θ . The variables are written as

$$f(r, \theta, z, t) = \sum_{m=-m_{\max}}^{m_{\max}} f_m(r, z, t) e^{im\theta}, \quad (2.6)$$

where f denotes one of $\{u, v, w, p\}$. To provide adequate accuracy for the parameter regimes studied here, we use $m_{\max} = 8$, and uniform grids with discretization length $\delta r = \delta z = 0.05$ and time steps $\delta t < 1/3800$.

A. Symmetries

In the absence of any external applied magnetic field, the finite Taylor-Couette system, where the fluid is confined by end walls, is invariant to arbitrary rotations about the axis and the reflections about axial midheight. With an imposed transverse magnetic field, these symmetries are broken and the flow is inherently three-dimensional for any nonzero Re and s_x , as a result of the rotating inner cylinder with the transverse magnetic field. As discussed in Ref. [21], the only $m = 2$ mode contribution is stimulated. Likewise, a pure axial magnetic field does not stimulate any further mode contributions. With the outer cylinder at rest and with the rotating inner cylinder in a clockwise direction (from the top of the system), the interaction of the magnetic terms in the ferrohydrodynamic equation results in a downward directed force on the side, where the field enters the system ($\varphi = 0$), and an upward directed force on the opposite side ($\varphi = \pi$), where the field exits the annulus. Thus, the resultant flow provides complex symmetries. There is the reflection K_z^H about the annulus' midheight plane along with an inversion of the magnetic field direction and the rotation invariance R_α^H for discrete angle $\alpha = \pi$ along with an inversion of the magnetic-field direction. Here the angle π is just aligned with the direction of the magnetic field to enter the annulus. The actions of these symmetries on the velocity fields are

$$\begin{aligned} R_\pi^H(u, v, w, H)(r, \theta, z) &= (u, v, w, -H)(r, \theta + \pi, z), \\ K_z^H(u, v, w, H)(r, \theta, z) &= (u, v, -w, -H)(r, \theta, -z). \end{aligned} \quad (2.7)$$

This gives the identical transformation and action,

$$R_\pi^H \text{LW} = \text{LW},$$

where LW (RW) indicates left-winding (right-winding) characteristics in the azimuthal wave number $m = 2$, respectively

(cf. Sec. III A). Thus, this rotation action does not affect the solutions. Due to the reflection action, the left-winding solution may change the right-winding one or vice versa, i.e.,

$$K_z^H \text{LW} = \text{RW}.$$

Therefore, corresponding LW and RW solutions have identical modal kinetic energies. In this paper, if not explicitly explained, we will just consider one, mostly the LW solution.

III. BASIC FLOWS

A. Pattern formation with s_x

First of all, we discuss the influence of the transverse magnetic field with $\lambda_2 = 0$. To investigate the flow modification of the magnetic field, we consider the difference between the azimuthal vorticity associated with flow states with and without any magnetic field, i.e.,

$$\Delta\eta := \eta(s_x) - \eta(s_x = 0).$$

Figure 1 shows isosurfaces of $\Delta\eta$ by increasing the transverse magnetic-field strength s_x as indicated. The top row in Fig. 1 shows the full solutions while the bottom row is of

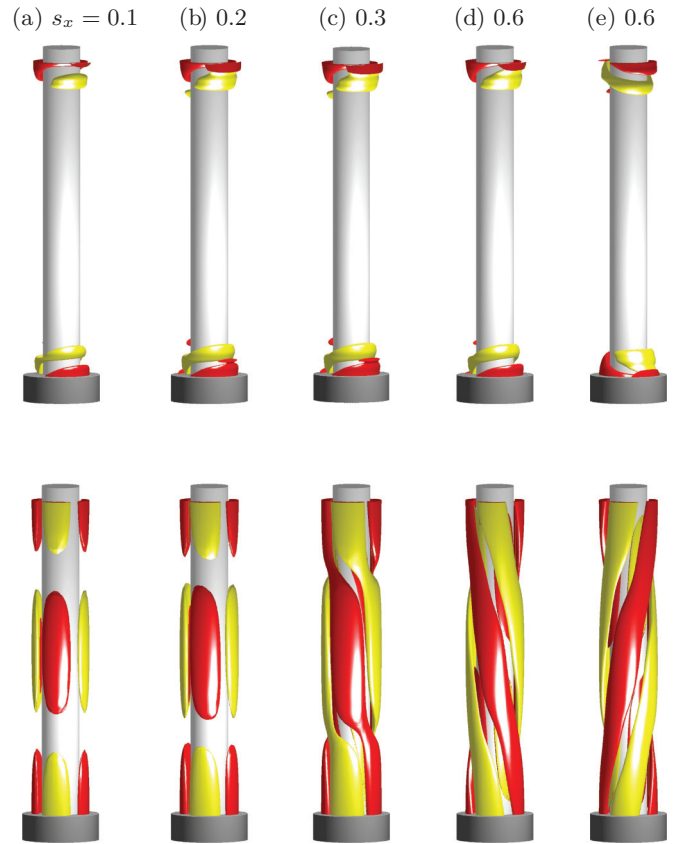


FIG. 1. (Color online) Isosurfaces of $\Delta\eta = \eta(s_x) - \eta(s_x = 0)$ for LW (a)–(d) and RW (e) at $\text{Re} = 60$, $\lambda_2 = 0$, and different transverse magnetic-field strengths s_x as indicated. The top row shows differences of the full solution [isolevel shown at $\Delta\eta = \pm 0.06$ (a), ± 0.08 (b) and (c), and ± 2 (d) and (e)] and the bottom row is of the $m = 2$ contributions [isolevel shown at $\Delta\eta = \pm 0.001$ (a), ± 0.003 (b) and (c), and ± 0.03 (d) and (e)]. Note that (e) gives the RW at the same parameters as the LW shown in (d). Red (dark gray) [yellow (light gray)] indicates positive (negative) values.

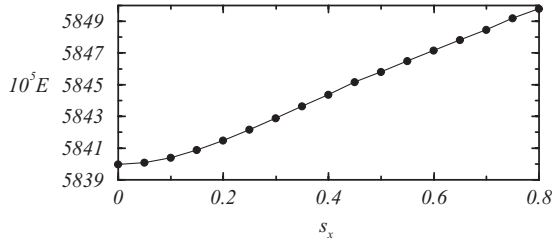


FIG. 2. Variation of the total modal kinetic energy E vs s_x for $\text{Re} = 60$ and $\lambda_2 = 0$. Note that the energy is identical for LW and RW.

$m = 2$ contributions. Obviously, due to the finite transverse magnetic field, the basic state is changed. In particular, the strengthened $m = 2$ azimuthal component modifies the flow pattern in the whole bulk. Here, the $m = 2$ azimuthal component contributes either LW or RW symmetrically related to each other. These states are stationary by being pinned into the position of the imposed transverse magnetic field which generates them. In Fig. 1, we only present the LW solutions, except in part (e), which gives the RW under the same parameter setting for the LW shown in (d). Under the influence of the transverse magnetic field, such a degenerated basic state with different helicity in Taylor-Couette flow based on the symmetry breaking has not been previously reported.

For the basic state, Fig. 2 shows the variation of the total modal kinetic energy E (as a global measure) versus s_x :

$$E := \sum_m E_m = \int_0^{2\pi} \int_{-\Gamma/2}^{\Gamma/2} \int_{r_i}^{r_o} \mathbf{u}_m \mathbf{u}_m^* r \, dr \, dz \, d\theta, \quad (3.1)$$

where \mathbf{u}_m is the m th Fourier mode of the velocity field. In both cases of LW and RW, the total modal kinetic energy E is the same. This implies that there is a symmetry relation.

B. Flow modifications under elongational flow

To understand the influence of elongational flow ($\lambda_2 \neq 0$), we will investigate the flow modification generated by the transverse magnetic field with $\lambda_2 \neq 0$. In the absence of λ_2 , the magnetic-field dependence s_x affects the flow modification, as shown in Fig. 1. That is, for small s_x , the flow pattern is almost reflection-symmetric, as shown in Fig. 1(a), but for stronger s_x , we can see the helical shape in the $m = 2$ azimuthal component, as shown in Figs. 1(d) and 1(e). Thus, we will focus on comparable cases with small and strong magnetic-field strengths s_x . As a comparable or reference solution to check the effect of elongational flow, we will consider the LW solution shown in Fig. 1(a) with $s_x = 0.1$, and then examine the difference in the azimuthal vorticity before and after applying the finite transport coefficient λ_2 :

$$\Delta_2 \eta := \eta(\lambda_2 \neq 0) - \eta(\lambda_2 = 0). \quad (3.2)$$

To investigate the influence of a small magnetic-field strength with a finite transport coefficient, for the fixed $s_x = 0.1$, Fig. 3 shows the isosurface of $\Delta_2 \eta$ for the transport coefficient dependence λ_2 [top row for the difference $\Delta_2 \eta$ in azimuthal vorticity of the full solution and bottom row for the difference $\Delta_2 \eta(m = 2)$ in azimuthal vorticity for the $m = 2$ azimuthal

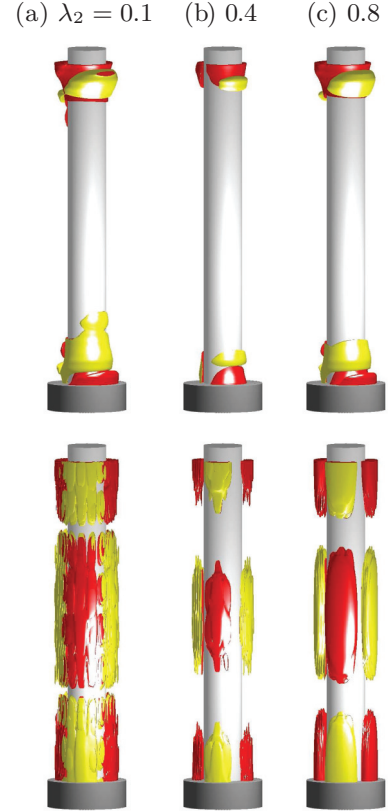


FIG. 3. (Color online) Isosurfaces of $\Delta_2 \eta = \eta(\lambda_2 \neq 0) - \eta(\lambda_2 = 0)$ for LW at $\text{Re} = 60$, $s_x = 0.1$, and λ_2 as indicated. The top row is of the full solution [isosurface shown at (a) $\Delta_2 \eta = \pm 0.005$ and (b) and (c) ± 0.05] and the bottom row is of the $m = 2$ contributions [isosurface shown at $\Delta_2 \eta$ (a) $\pm 1.12 \times 10^{-5}$ and (b) and (c) $\pm 5.2 \times 10^{-4}$].

component]. The variation of the magnitudes for the isosurface of plotted surfaces is finite, but quite small (cf. also Fig. 4). It is also satisfied for both cases [$\Delta_2 \eta$, $\Delta_2 \eta(m = 2)$]. For such small magnetic-field strength s_x with finite λ_2 , we see that the flow is modified in the whole interior of the bulk. But the

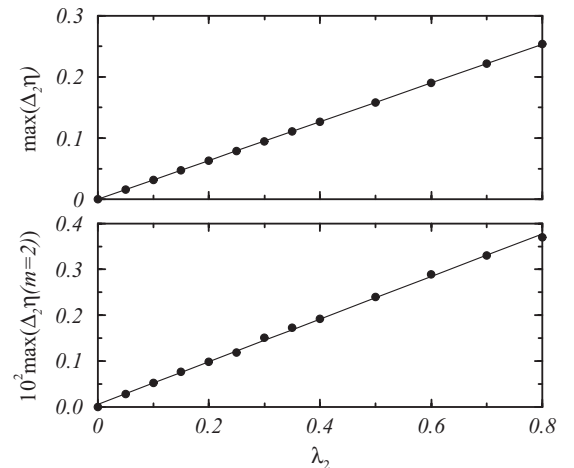


FIG. 4. Variation of $\max(\Delta_2 \eta)$ and $\max[\Delta_2 \eta(m = 2)]$ for LW vs λ_2 for $\text{Re} = 60$ and $s_x = 0.1$. Lines are linear fits.

important fact is that its symmetry is not affected. When figures are compared in the sense of the $m = 2$ azimuthal component, i.e., the bottom row of Fig. 3 and the bottom row of Fig. 1(a), they are very similar in color and shape. Thus, at least for these control parameters ($s_x = 0.1$ with $\lambda_2 \neq 0$), the effect of the magnetic-field strength s_x will be enforced by a finite λ_2 .

Figure 4 shows how the maxima of $\Delta_2\eta$ and $\Delta_2\eta(m=2)$ vary with λ_2 . Although the maxima of these values are significantly different, they are linearly scaled with λ_2 starting at zero. Lines in Fig. 4 are calculated by linear regression fitting for the numerical data.

From the bottom row of Figs. 1(c)–1(e), we can see that the helical symmetry in the $m = 2$ azimuthal component is much more pronounced even in a larger magnetic-field strength. To investigate the influence of finite λ_2 for such a larger magnetic-field strength, we will consider the parameter setting and the flow shown in Fig. 1(d) as the initial solution, which has a left-winding symmetry in the $m = 2$ azimuthal component.

For a fixed magnetic-field strength $s_x = 0.6$ (or a larger magnetic-field strength), Fig. 5 shows isosurfaces of azimuthal vorticity differences, $\Delta_2\eta$ and $\Delta_2\eta(m=2)$, with a different finite transport coefficient λ_2 (top row for the full solution and bottom row for $m = 2$ contributions). The top row in Fig. 5 shows that the flow modification of the full field occurs locally

near the Ekman boundary layers, and then by increasing λ_2 it strengthens more into the bulk. In the sense of the $m = 2$ azimuthal component, the flow is modified into the whole interior of the bulk under the influence of a finite λ_2 , as shown in the bottom row of Fig. 5. It is very similar to the case of an applied transverse magnetic field with $\lambda_2 = 0$, compared to Fig. 1. Therefore, it implies that the modification of flow becomes more pronounced by enlarging λ_2 .

By comparing Figs. 1(a) and 3, we can say that the transport coefficient dependence in a small magnetic-field strength is very weak, because the flow modified by λ_2 almost coincides with Fig. 1(a) when comparing the color indicated in the figures. However, in the shape of the modified flows, it is changed and more complicated.

For the dependency of the transport coefficient in large magnetic-field strength, the flow modification keeps the helical left-winding symmetry in the $m = 2$ contribution if the transport coefficient is comparable small, as shown in Figs. 5(a)–5(c). But, for a larger transport coefficient, see Figs. 5(d) and 5(e), we can see that there is a switch from left- to right-winding even when starting the left-winding solution ($\lambda_2 = 0$) as the initial state [cf. Fig. 1(d)]. This means that in the flow pattern, the transport coefficient λ_2 will increase right-winding symmetry over the $m = 2$ azimuthal component when the left-winding solution is taken as the initial solution. That is, in the absence of λ_2 , the left-winding symmetry remains in the transverse magnetic field, but due to the influence of the finite transport coefficient λ_2 , azimuthal mode-2 can have stronger left- or right-winding characteristics. In addition, when taking a right-winding solution as the initial state [Fig. 1(e)], the flow pattern over azimuthal mode-2 is also modified in the same way. This is a qualitative characteristic of the flow modification in the transverse magnetic field with a large transport coefficient. Here, all flow patterns are stationary without any rotation.

Figure 6 shows how the variation of $\max(\Delta_2\eta)$ and $\max[\Delta_2\eta(m=2)]$ for the left-winding solution changes with λ_2 . All curves in Fig. 6 are linearly scaled with λ_2 starting at zero. So, for the modification of the basic state in the transverse magnetic field, the transport coefficient or elongational flow linearly influences the $m = 2$ azimuthal symmetry.

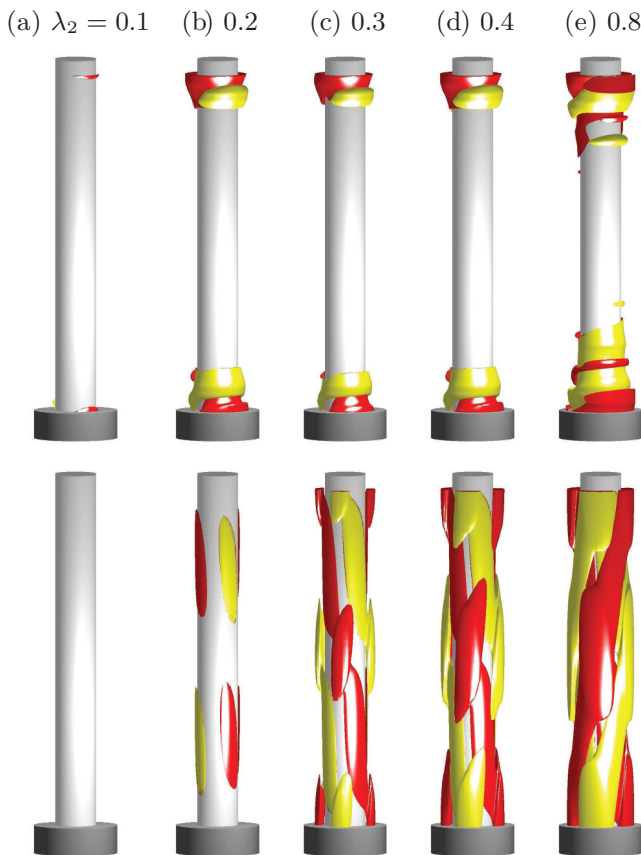


FIG. 5. (Color online) Isosurfaces of $\Delta_2\eta = \eta(\lambda_2 \neq 0) - \eta(\lambda_2 = 0)$ for LW at $\text{Re} = 60$, $s_x = 0.6$, and λ_2 as indicated. The top row is of the full solution (isolevel shown at $\Delta_2\eta = \pm 1$) and the bottom row is of the $m = 2$ contributions (isolevel shown at $\Delta_2\eta = \pm 0.02$).

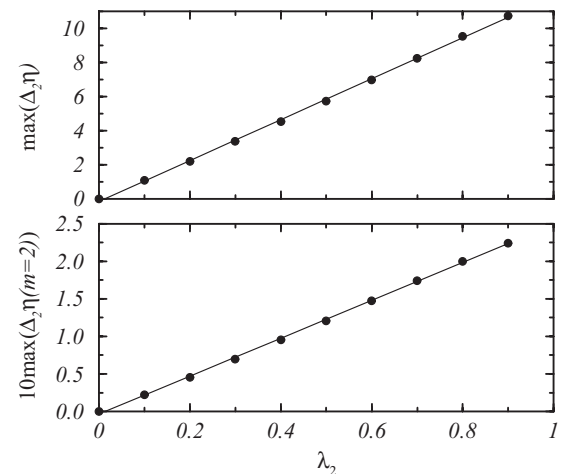


FIG. 6. Variation of $\max(\Delta_2\eta)$ and $\max[\Delta_2\eta(m=2)]$ for LW vs λ_2 at $\text{Re} = 60$ and $s_x = 0.6$ (cf. Fig. 5). Lines are linear fits.

IV. SUPERCRITICAL SOLUTIONS—FLOW INSTABILITIES

A. Bifurcation thresholds

Many numerical and experimental works on ferrofluids show a stabilizing effect of the magnetic field on the basic state by shifting bifurcation thresholds of supercritical flow states in control parameters [7,18,20–23]. This effect is also satisfied in periodic and rigid boundary conditions, as is supposed in this paper. While an axial magnetic field does not change the flow, a transverse magnetic field breaks axisymmetry and leads to several nonlinear effects because it “modulates” the flow structures found in the absence of a magnetic field or in the presence of an axisymmetric field. For instance, the supercritical flow of a wavy Taylor vortex flow (wTVF) can be generated by a Taylor vortex flow (TVF) under the influence of a transverse magnetic field [7,20,21]. This new flow structure differs qualitatively from the classical flows found in the absence of the magnetic field. When a transverse magnetic field is applied to centrifugal unstable flows, we will investigate the effect of elongational flow. Note that due to the orientation of the magnetic field, the bifurcating solutions with $s_x \neq 0$ are modified into the wavy Taylor vortex flow [7,20,21] instead of a classical Taylor vortex flow with $s_x = 0$ and any s_z .

To quantitatively compare our numerical results to experimental findings, we will consider the experimental result [7] for the ferrofluid in the Taylor-Couette system in the presence of an axial magnetic field instead of a transverse magnetic field due to the lack of experimental results in a transverse magnetic field. Figure 7 presents the onsets of centrifugal unstable flows (TVF and wTVF) under the influence of a transverse or an axial magnetic field with λ_2 . Both short horizontal lines shown in Fig. 7 indicate the experimental onsets [7] at $\text{Re}_c(s_z = 0.233) = 74.68$ and $\text{Re}_c(s_z = 0.409) = 79.47$, respectively, where Re_c stands for the critical value. Comparing these cuts to our numerical results, we qualitatively find that the value of λ_2 will be about 0.2. This value for a transport coefficient is also in agreement with further experimental measurement [9].

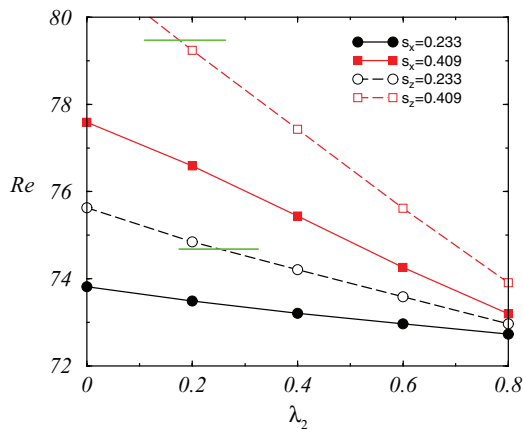


FIG. 7. (Color online) For different field strengths s_x , variation of the onsets of centrifugal unstable flows (TVF for $s_x = 0$ and wTVF) for Re vs λ_2 . Lines are linear fits. Points are just to guide the eyes; the numerical calculations are done for a larger number of points. Both short horizontal lines indicate the experimentally obtained onsets [7] [$\text{Re}_c(s_z = 0.233) = 74.68$ and $\text{Re}_c(s_z = 0.409) = 79.47$].

In addition, Fig. 7 indicates that the shift in the bifurcation threshold under the axial magnetic field is larger than that of the transverse magnetic field.

Considering the effect of elongational flow, the critical bifurcating point of primary centrifugal instability will be shifted. By increasing λ_2 , the critical point for the onset of centrifugal instability is moved to lower Re . Comparing the situation without having elongational flow, the flow below the centrifugal instability becomes less stabilized in the magnetic field. Therefore, by increasing either a transverse s_x or an axial s_z field strength, a similar situation can be found qualitatively. This means that here the additional term *counteracts* the general stabilization in any magnetic field which remains *untouched*. As is pointed out after the discussion in Sec. III, the basic flow is either a left-winding or a right-winding solution. However, the general bifurcation behavior of the flow, other than centrifugal instability, remains unaffected as a supercritical Hopf bifurcation.

We remark that (i) when applying a magnetic field into a basic state, a general stabilization behavior remains *untouched* and flow modification depends linearly on λ_2 , (ii) due to λ_2 , the axial wave number k corresponding to the used bulk length can be enforced or damped by the flow modifications, and (iii) both the Niklas approximation theory and the properties of the used ferrofluid [9] may play a significant role in stabilizing the basic state.

B. Wave-number selection

We will consider a classical Taylor vortex flow as the initial flow state, with $n = 22$ vortices corresponding to an axial wave number $k = 3.41$ in the bulk, which can be seen in the left border in Fig. 8. By increasing the magnetic-field strength, s_x , the number of vortices is reduced, which leads to an increase in the wavelength. Therefore, the axial wave number k in the bulk can be reduced. Note that, as shown in Fig. 8, the wavylike modulation is not visible. The exact field strength s_x for vortex elimination or the number of destroyed vortices depends on λ_2 .

In the case in which $\lambda_2 = 0$ and $s_x = 0$, the flow has 22 vortices with an axial wave number $k = 3.41$. Until the parameter s_x approximately reaches the value 0.7, the flow remains stable, but the number of vortices in the flow can be reduced to $n = 20$ with $k = 3.04$. By increasing the number s_x to 0.85, the number of vortices can be more reduced to $n = 16$ with $k = 2.58$. However, before reaching the boundary threshold ($s_x \approx 0.9$), there is no change in the number of vortices.

When $\lambda_2 = 0.2$, the behavior of the vortex state is similar to the case neglecting elongational flow effects ($\lambda = 0$) and it remains stable before the parameter s_x reaches 0.75. But the number of vortices is also reduced to $n = 20$ with $k = 3.04$. Until the parameter s_x increases the boundary threshold ($s_x \approx 0.95$), the number of vortices remains unchanged. In the case in which $\lambda_2 \gtrsim 0.7$, the solution is not affected by the magnetic-field strength. There is a flow with $n = 22$ vortices corresponding to an axial wave number $k = 3.41$ in the bulk. There is an interesting phenomenon that one or two vortex pairs can be eliminated. This can be seen in the experimental result [7], but there is no physical explanation so far. We also find a similar reduction scenario for pure axial magnetic fields. This can correspond to the strength of λ_2 with a larger reduction.

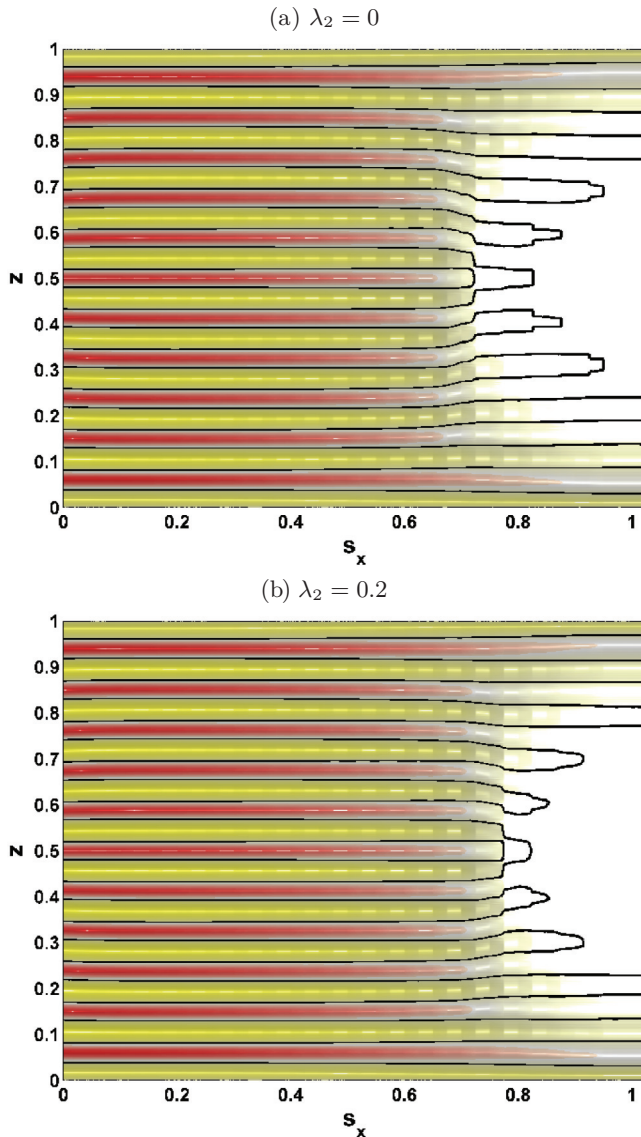


FIG. 8. (Color online) Contours of the radial velocity component u at midgap with variation of field strength s_x at $\text{Re} = 88.35$ and λ_2 as indicated. The initial state at the left border in each plot is a classical Taylor vortex flow with $n = 22$ vortices corresponding to an axial wave number $k = 3.41$ in the bulk. Note that for $s_x \neq 0$, only wavylike modified flow states exist. Red (yellow) [dark gray (light gray)] corresponds to positive (negative) values. The max (min) level is ± 9.98 .

C. Flow pattern modifications on supercritical flow due to λ_2

In this section, the effect of elongational flow on the structure of supercritical flow will be investigated. Regarding the effect of elongational flow with a finite quantity λ_2 on the basic state, we already showed that the flow is linearly modified and the shape of the flow patterns can be changed in the same way when the magnetic field is applied. Therefore, the transport coefficient λ_2 can be aligned or counteracted with the flow modification of the magnetic field. This implies that the elongational flow will enhance the effect of the magnetic field.

Now, we will investigate the flow modifications of centrifugal unstable flows under the influence of elongational flow ($\lambda_2 \neq 0$). For a fixed field strength $s_x = 0.1$ and several

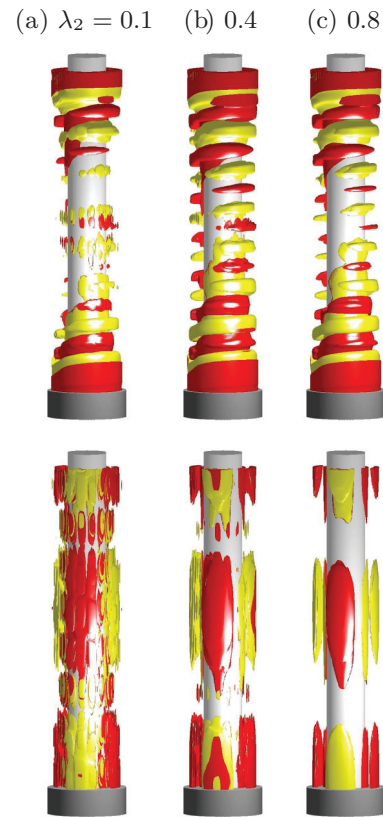


FIG. 9. (Color online) Isosurfaces of $\Delta_2\eta = \eta(\lambda_2 \neq 0) - \eta(\lambda_2 = 0)$ for flow at $\text{Re} = 100$, $s_x = 0.1$, and λ_2 as indicated. The top row is of the full solution [isolevel shown at (a) $\Delta_2\eta = \pm 0.003$, (b) ± 0.007 , and (c) ± 0.015] and the bottom row is of the $m = 2$ contributions [isolevel shown at $\Delta_2\eta$ (a) $\pm 2 \times 10^{-4}$, (b) $\pm 2.5 \times 10^{-4}$, and (c) ± 0.001].

finite λ_2 , Fig. 9 shows the isosurfaces for $\Delta_2\eta$ and $\Delta_2\eta(m = 2)$ as the effect of elongational flow on supercritical flow. A comparison of the isosurfaces in Figs. 5 and 9 suggests that the effect of finite λ_2 is almost the same, but the modification within the bulk is much different due to the fact that visible isosurfaces over the whole bulk length are much stronger. Figure 10 shows again a linear scaling with λ_2 starting at zero (cf. Fig. 6). However, values of $\max[\Delta_2\eta(m = 2)]$ are significantly larger. This is due to the already existing strong flow pattern in the interior when $\lambda_2 = 0$. Again, the mode-2 symmetries are conserved and all flows are stationary nonrotating solutions.

In the case of a stronger field strength, as shown in Fig. 11, there is an opposite helical contribution in the azimuthal mode-2, which is significantly enforced by the influence of λ_2 , compared with Fig. 3 for the LW basic state. In addition, a wavylike modulation of the vortices in the azimuthal direction can be observed that results from the transverse field. All vortices become tipped out of its horizontal plane.

Under the influence of elongational flow on basic state and supercritical unstable flows, the maximal vorticity $\max(\Delta_2\eta)$ varies linearly, but the maximal vorticity in the azimuthal mode-2, $\max[\Delta_2\eta(m = 2)]$, is significantly smaller, as shown in Fig. 12.

From Figs. 9 and 11, the vortex tipping is obviously observed. Both cases illustrate that the Taylor vortices are

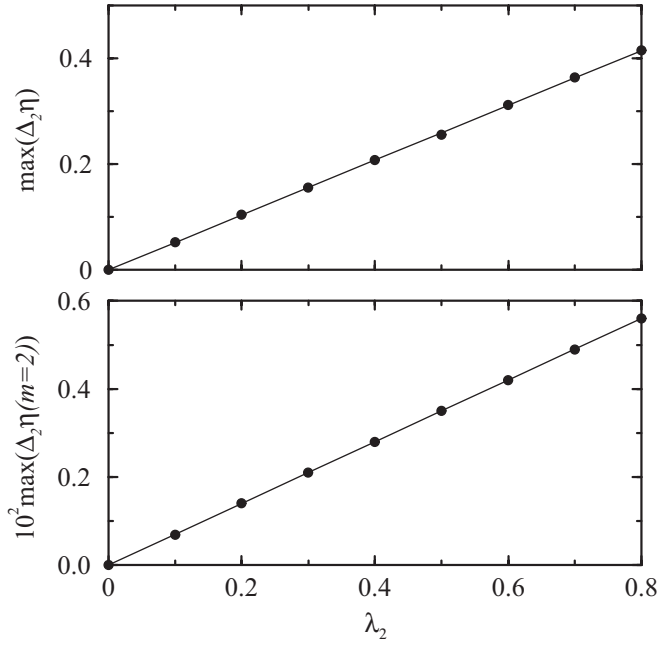


FIG. 10. Variation of $\max(\Delta_2 \eta)$ and $\max[\Delta_2 \eta (m=2)]$ vs λ_2 for supercritical flow at $\text{Re} = 100$ and $s_x = 0.1$. Lines are linear fits.

tilted downward (upward) when the magnetic field approaches (leaves) the annulus, respectively. It directly comes from the combination of the inner cylinder rotation and the transverse magnetic field, as discussed in Sec. II.

D. Radial gradients of angular momentum balance

In this section, we will consider the case in which the outer cylinder is nonstationary. In particular, for co- and counterrotating outer cylinders, their rotation rates $\omega r_2 d / \nu$ are 40 and -40 , respectively. To measure the effect of elongational flow, we will consider the radial gradient of angular momentum, $G = \partial(rv)/\partial r$. For a quantitative comparison of various control parameters, we will use the reduced quantity, $\Delta_G(r) = G(r, s_x, \lambda_2) / G(r, s_x = 0) - 1$.

In Fig. 13, the variations of basic states in the co- and counterrotation cases are shown as $\Delta_G(r)$ versus r for different field strengths s_x and λ_2 . For $\lambda_2 = 0$, $\Delta_G(r)$ is almost zero for any field strength $s_x \neq 0$. Therefore, we did not show it in Fig. 13, but for $\lambda_2 \neq 0$, there is a measurable difference in $\Delta_G(r)$. By increasing λ_2 , Figs. 13(a)–13(d) show the amplitude modification of $\Delta_G(r)$ over the gap width. In the case of corotating cylinders, Δ_G increases near the cylinder walls and decreases in the middle of the bulk for $\lambda_2 \neq 0$. But, in the case of counterrotating cylinders, Δ_G is maximized at the interior and reduced near the walls for $\lambda_2 \neq 0$. In general, the flow modification becomes enlarged by increasing λ_2 and also is stronger in the case of counterrotating cylinders. In addition, we find that all curves shown in Fig. 13 have qualitatively the same behavior even for different field strengths s_x .

Mathematically, the effect of elongational flow can be explained by a direct coupling of λ_2 and nonlinear terms in the equations, which can increase the magnetic field parameter s_x . As a physical interpretation for the effect of elongational flow, when increasing the magnetic field strength, particle-particle

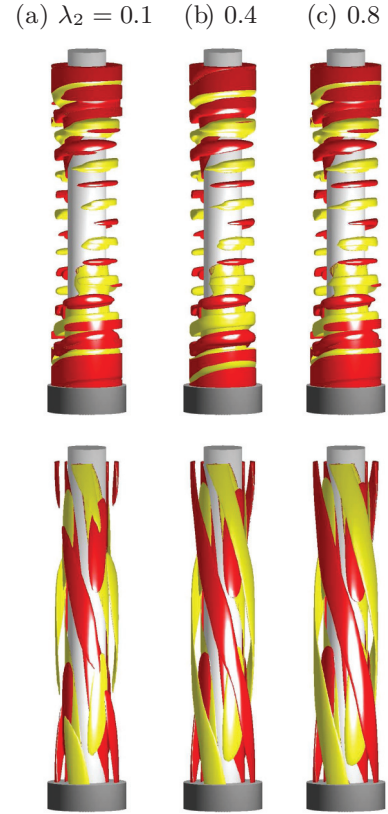


FIG. 11. (Color online) Isosurfaces of $\Delta_2 \eta = \eta(\lambda_2 \neq 0) - \eta(\lambda_2 = 0)$ for supercritical flow at $\text{Re} = 100$, $s_x = 0.6$, and λ_2 as indicated. The top row is of the full solution [isolevel shown at (a) $\Delta_2 \eta = \pm 0.1$, (b) ± 0.4 , and (c) ± 0.7] and the bottom row is of the $m = 2$ contributions [isolevel shown at $\Delta_2 \eta$ (a) ± 0.01 , (b) ± 0.04 , and (c) ± 0.07].

interaction will be increased due to the influence of the finite volume particles. This means that the chain-building process is more significant [6,15], and so the strength of elongational flow increases.

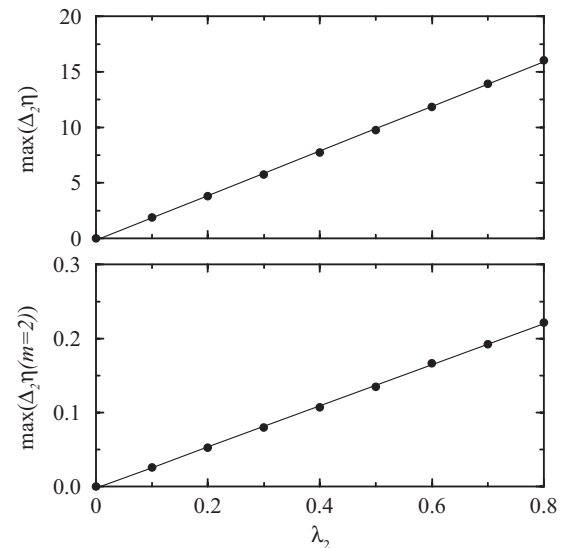


FIG. 12. Variation of $\max(\Delta_2 \eta)$ and $\max[\Delta_2 \eta (m=2)]$ vs λ_2 for flow at $\text{Re} = 100$ and $s_x = 0.6$. Lines are linear fits.

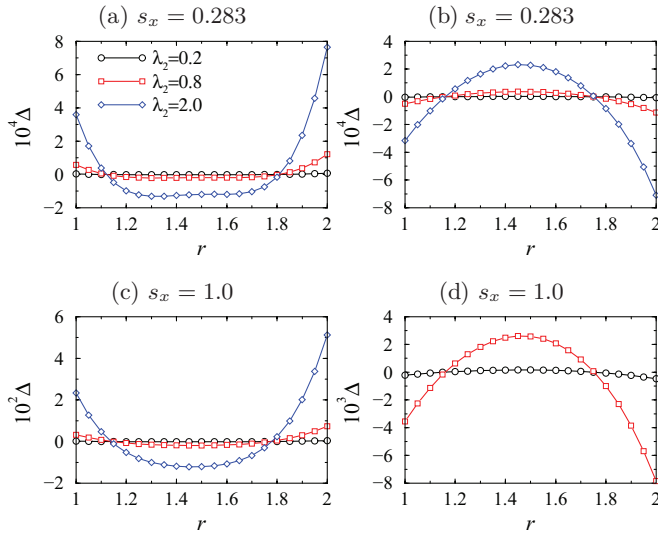


FIG. 13. (Color online) Influence of λ_2 on the radial gradient of angular momentum G of the basic state for a system with outer cylinder corotation $\omega r_2 d / \nu = 40$ (a) and (c) and counterrotation $\omega r_2 d / \nu = -40$ (b) and (d) for $\text{Re} = 40$. Variation of $\Delta_G(r) = G(r, s_x, \lambda_2) / G(r, s_x = 0) - 1$ vs r for s_x and λ_2 as indicated. In (d), the curve for $\lambda_2 = 2$ is missed due to the shift of the onset, i.e., the supercritical flow already existed.

Note that, as shown in Fig. 13, although the modification $\Delta_G(r)$ of flow states in the presence of λ_2 is small and finite, the shape of the flow is almost unchanged for any λ_2 and is only enforced in a linear manner (cf. Sec. III B).

V. CONCLUSION AND DISCUSSION

To explore the effect of elongational flow on ferrofluid in the presence of the transverse or the axial magnetic field, we consider the so-called *transport coefficient* λ_2 on the Taylor-Couette system with stationary, nonrotating, rigid end walls and an outer cylinder mostly at rest. To numerically study the effect of elongational flow, the nondimensional governing equations including the transport coefficient are presented. Elongational flow can be incorporated by the symmetric part of the velocity gradient field tensor in the nondimensional governing equations, which can be scaled by the transport coefficient λ_2 . Mathematically, the transport coefficient λ_2 can be described in the symmetric part of the velocity gradient of the ferrohydrodynamic equations of motion. To do direct numerical simulations, we assume a stationary magnetization near equilibrium and a sufficiently small relaxation time including the λ_2 term in the magnetization equations. It is a similar approach to that shown in the model of Niklas *et al.* [18,19,21].

In the case of $\lambda_2 = 0$, the classical system's symmetries are broken for a finite transverse magnetic field $H_x \neq 0$, and so the flow is inherently three-dimensional. Actually, the resulting flow has a helical shape that is either left-winding or right-winding in the sense of the azimuthal mode-2. Thus, the flow remains a stationary state being pinned into position due to the imposed magnetic field which generates it.

For a finite transport coefficient, i.e., $\lambda_2 \neq 0$ or due to the effect of elongational flow, we find that the shape of the flow pattern is not qualitatively modified and the flow modification can be linearly enforced by keeping the symmetry in the sense of the azimuthal mode-2. Additionally, it holds for both the basic flow and the primary instability—a supercritical centrifugal unstable flow. We also find the well-known *stabilization effect* for any magnetic field, which is known because the onset of centrifugal instability is relatively shifted in the bifurcation curve [7,20,21,23]. Depending on various system parameters (for instance, the axial wave number k and the cylinder rotation rate), the stabilization effect can be either *stronger* or *weaker*. Thus, under the influence of a magnetic field, elongational flow ($\lambda_2 \neq 0$) can enforce or dampen the flow stabilization, which remains untouched. In general, we can say that elongational flow enhances the effect of magnetic fields. Physically, we may say that particle-particle interaction and the chain formed by the flow of the fluid are more significantly influenced due to the increasing magnetic-field strength. This implies that modifications of the spatiotemporal structure can happen, especially for the basic state and the centrifugal unstable flow.

For a qualitative and quantitative comparison between our numerical results and experimental findings, we consider the bifurcation thresholds of centrifugal unstable flow under the influence of the axial magnetic field [7], and we find very good agreement with the value of the transport coefficient λ_2 , which is about 0.2. This value is observed in Ref. [15]. As another measurement for the effect of λ_2 , we consider the radial gradient of angular momentum G . For different field strengths s_x , G is changed, but it is qualitatively similar by increasing λ_2 . In the case of corotating inner and outer cylinders, the radial gradient of angular momentum G is minimized in the middle of the bulk, but it is increased near the cylinder walls due to the effect of elongational flow. However, in the case of counterrotating inner and outer cylinders, the reverse phenomenon is true for G . In general, for strong elongational flow, this phenomenon is stronger, especially for counterrotating cylinders.

ACKNOWLEDGMENTS

This work was supported by WCU (World Class University) program through the Korea Science and Engineering Foundation funded by the Ministry of Education, Science and Technology (Grant No. R32-2009-580 000-20021-0).

- [1] R. E. Rosensweig, *Ferrohydrodynamics* (Cambridge University Press, Cambridge, 1985).
 [2] J. E. Hart, *Dyn. Atmos. Oceans* **41**, 121 (2006).
 [3] J. E. Hart and S. Kittelman, *Dyn. Atmos. Oceans* **41**, 139 (2006).

- [4] M. I. Shliomis, *Sov. Phys. JETP* **34**, 1291 (1972).
 [5] J. P. McTague, *J. Chem. Phys.* **51**, 133 (1969).
 [6] S. Odenbach and H. W. Müller, *J. Magn. Magn. Mater.* **289**, 242 (2005).

- [7] M. Reindl and S. Odenbach, *Phys. Fluids* **23**, 093102 (2011).
- [8] S. Mahle, P. Ilg, and M. Liu, *Phys. Rev. E* **77**, 016305 (2008).
- [9] H. W. Müller and M. Liu, *Phys. Rev. E* **64**, 061405 (2001).
- [10] P. J. W. Debye, *Polar Molecules* (Dover, New York, 1929).
- [11] M. A. Martsenyuk, Y. L. Raikher, and M. I. Shliomis, *Sov. Phys. JETP* **38**, 413 (1974).
- [12] *The Physics of Liquid Crystals*, edited by G. P. Gilles de and J. Prost (Clarendon, Oxford, 1983).
- [13] F. Gazeau, B. M. Heegaard, J. C. Bacri, A. Cebers, and R. Perzynski, *Europhys. Lett.* **35**, 609 (1996).
- [14] F. Gazeau, C. Baravian, J. C. Bacri, R. Perzynski, and M. I. Shliomis, *Phys. Rev. E* **56**, 614 (1997).
- [15] S. Odenbach and H. W. Müller, *Phys. Rev. Lett.* **89**, 037202 (2002).
- [16] P. Langevin, *Ann. Chem. Phys.* **5**, 70 (1905).
- [17] J. Embs, H. W. Müller, C. Wagner, K. Knorr, and M. Lücke, *Phys. Rev. E* **61**, R2196 (2000).
- [18] M. Niklas, *Z. Phys. B* **68**, 493 (1987).
- [19] M. Niklas, H. Müller-Krumbhaar, and M. Lücke, *J. Magn. Magn. Mater.* **81**, 29 (1989).
- [20] S. Altmeyer, J. Lopez, and Y. Do, *Phys. Rev. E* **85**, 066314 (2012).
- [21] S. Altmeyer, C. Hoffmann, A. Leschhorn, and M. Lücke, *Phys. Rev. E* **82**, 016321 (2010).
- [22] A. Leschhorn, M. Lücke, C. Hoffmann, and S. Altmeyer, *Phys. Rev. E* **79**, 036308 (2009).
- [23] M. Reindl and S. Odenbach, *Exp. Fluids* **50**, 375 (2011).
- [24] A. Yu. Zubarev and Yu. Skakova, *Phys. Rev. E* **61**, 5415 (2000).
- [25] S. Altmeyer, A. Leschhorn, Ch. Hoffmann, and M. Lücke, *Phys. Rev. E* **87**, 053010 (2013).